24 Atomic Collisions in Matter

J. Keinonen

Department of Physical Sciences, Accelerator Laboratory, P.O. Box 43, 00014
University of Helsinki, Finland

24.1 Introduction

Energetic ions (in the energy range from the eV region to the MeV region considered in this chapter) collide with electrons and nuclei when penetrating into materials. In solid matter, the energy loss of ions is connected to the first-order effects on the atoms of the material, particularly the electronic excitation and displacement of lattice atoms, and the production of plasmons and phonons. The trajectory of an ion is determined by successive inelastic and elastic binary encounters with the lattice atoms. The implantation of ions results in a distribution of stopped ions and damage. In addition to the ion irradiation and implantation of materials, atomic collisions are utilized in methods of ion beam analysis of materials, such as Rutherford backscattering spectrometry (RBS) and elastic recoil detection analysis (ERDA).

In this chapter, a basic formalism is used to illustrate collisions of ions with atoms, i.e. their nuclei and electrons. Then some phenomena in atomic collisions for ions penetrating into materials are described. Finally, effects in materials caused by the impinging ions are discussed. Computer methods used to calculate the slowing down of ions, and interatomic potentials defining the force between nuclei of the ion and target atom are described in two appendixes.

24.2 Slowing Down of Energetic Ions

The stopping of energetic heavy ions in matter has received much theoretical and experimental interest for decades. Bohr's theory [1] of the stopping of charged particles in matter was extended by him [2] to point out the importance of screening due to projectile electrons in the slowing down of fission fragments. Since the appearance of the theory by Lindhard, Scharff, and Schiøtt (LSS theory) [3], heavy-ion stopping has commonly been divided into three velocity regions. At low velocities, the stopping force is taken to be proportional to the ion velocity [4] and was described originally by the theories of Firsov [5] and Lindhard and Scharff [6]. At high velocities, the basis for stopping calculations is the Bethe formula [7]. At intermediate velocities around the stopping maximum, the stopping force is characterized

by a Bethe-type formula in conjunction with an effective ion charge. Brandt and Kitagawa [8] established an explicit connection between the ion charge and stopping force. The book by Ziegler, Biersack, and Littmark [9] covers the physical phenomena and history associated with the penetration of energetic ions into solids. More recently, the book edited by Smith et al. [10] has covered the theory, simulation, and applications of atom and ion collisions in solids and at surfaces.

Comparisons with experimental values have indicated that the predictions of the analytical models are not sufficiently accurate. Some recent models improving the accuracy of stopping calculations with numerical methods are the binary theory [11], the generalization of the Friedel sum rule [12] for non-crystalline targets, and the convolution approximation [13] for crystalline targets.

Analytical models of particle penetration rely on the use of statistical-physics methods and transport equations [14] for the slowing down of an ion in a homogeneous material. Successive collisions are assumed to be statistically independent. Since these equations can be solved only for a limited set of environments, computer simulations based on the binary-collision approximation (BCA) (for example in [9]) and molecular-dynamics (MD) techniques (see [10]) have become widely used; for the techniques, see Appendix 24.A.

In the basic description of the slowing down of energetic ions produced in an accelerator and forming a beam with an incident flux density n, the ions impinging on solid matter are scattered from atoms. For each energy E of the ion and energy T transferred to the atom, the differential of the scattering cross section $\sigma(E,T)$ gives the fraction of ions n_Ω scattered into a solid angle $\mathrm{d}\Omega$ from the incident flux, i.e. $\mathrm{d}\sigma(E,T) = \sigma(E,T)\,\mathrm{d}\Omega = n_\Omega/n$.

In a medium where atoms are distributed randomly with a density N, the cross section $\mathrm{d}\sigma(E,T)$ defines the probability $\mathrm{d}P(E,T)$ for a collision, i.e. $\mathrm{d}P(E,T) = N\Delta z\,\mathrm{d}\sigma(E,T)$, where Δz is the distance traversed by the ion. In a number of collisions, the average energy loss $\langle \Delta E \rangle$ is given by

$$\langle \Delta E \rangle = \int T\,\mathrm{d}P = -N\Delta z \int_{T_{\min}}^{T_{\max}} T\,\mathrm{d}\sigma \;, \tag{24.1}$$

where $T_{\min}$ and $T_{\max}$ are the minimum and maximum transferred energy, respectively. This equation defines the nuclear stopping power $(\mathrm{d}E/\mathrm{d}x)_{\mathrm{n}}$ and the stopping cross section $S_{\mathrm{n}}(E)$:

$$\left(\frac{\mathrm{d}E}{\mathrm{d}x}\right)_{\mathrm{n}} = -N \int T\,\mathrm{d}\sigma = -NS_{\mathrm{n}}(E) \;. \tag{24.2}$$

In addition to the energy loss in elastic collisions with atoms, the ions lose energy also in collision with electrons, in inelastic scattering of ions. This electronic stopping power is written in the form

$$\left(\frac{\mathrm{d}E}{\mathrm{d}x}\right)_{\mathrm{e}} = -NS_{\mathrm{e}}(E) \;. \tag{24.3}$$

If the nuclear and electronic stopping powers are independent, the total stopping power is

$$\frac{\mathrm{d}E}{\mathrm{d}x} = -N[S_\mathrm{n}(E) + S_\mathrm{e}(E)] \,. \tag{24.4}$$

The two main problems in the stopping theory are the calculation of $\sigma(E, T)$, and of the energy loss spectrum from that.

The nuclear and electronic stopping powers are illustrated in Fig. 24.1, where the stopping power is shown as a function of ion velocity for silicon ions slowing down in silicon. The crystalline structure is not taken into account in the calculations.

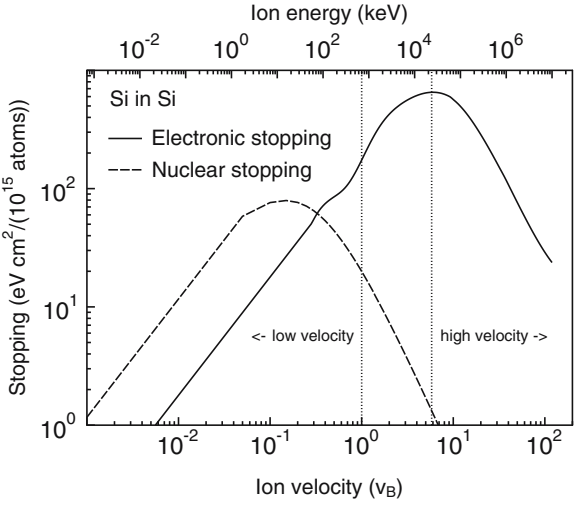

Fig. 24.1. Stopping powers for silicon ions slowing down in silicon as a function of the ion velocity. The velocity is given in the units of Bohr velocity v_B, namely the fine-structure constant of the atom times the velocity of light in vacuum. The stopping powers were calculated according to the empirical parametrization by Ziegler, Biersack, and Littmark by using the program SRIM [9]. The maximum of the electronic stopping power occurs at much higher velocities than that of the nuclear stopping. With decreasing velocity, the electronic stopping decreases before the nuclear stopping. This leads to the fact that for heavy ions, the nuclear stopping power dominates at low velocities

24.3 Collision of an Ion with an Atom

The basis for the description of collisions between impinging ions (atomic number Z_1, mass m_1) and electrons or nuclei of matter (atomic number Z_2, mass m_2) is the binary-collision approximation [9, 10]. A collision of an ion with a target atom and electron is described as a scattering in a central force field $F(r) = -\partial V(r)/\partial r$, where $V(r)$ is the central potential and r is the

distance between the ion and the target atom or electron. The basis of the interaction is the Coulomb potential $V(r) = Z_1 Z_2 e^2/r$. According to classical mechanics, the center-of-mass scattering angle θ is given by

$$\tan\frac{\theta}{2} = \frac{b}{2p}\,, \tag{24.5}$$

where p is the impact parameter (the distance of the extrapolated initial ion trajectory from the atom) and b is the collision diameter, defined by $Z_1 Z_2 e^2/b = MV^2/2$ for the reduced mass $m = m_1 m_2/(m_1 + m_2)$. If the target atom is assumed to be at rest initially, the energy loss deduced from conservation of energy and momentum is

$$T = T_{\max}\sin^2\frac{\theta}{2}\,, \tag{24.6}$$

where $T_{\max} = [4m_1 m_2/(m_1 + m_2)^2]E \equiv \eta E$. The differential scattering cross section is now $\mathrm{d}\sigma = \pi(b/2)^2(T_{\max}/T^2)\,\mathrm{d}T$, and the average energy loss according to (24.1) is

$$\langle \Delta E\rangle = N\Delta z\, 2\pi\frac{(Z_1 e)^2(Z_2 e)^2}{(m_2 v)^2}\ln\frac{T_{\max}}{T_{\min}}\,, \tag{24.7}$$

where $m_2 = m_{\mathrm{n}}$, the charge is $Z_2 e$, and $N = N_{\mathrm{n}}$ for the collisions with nuclei, and $m_2 = m_{\mathrm{e}}$, the charge is $-e$, and $N = Z_2 N_{\mathrm{n}}$ for the collisions with electrons. Equation (24.7) is based on the free-body scattering for ion velocities higher than the Bohr velocity v_{B}. It implies that for the same ion velocity, the electronic energy loss is much higher than the nuclear energy loss, i.e. $\langle \Delta E\rangle_{\mathrm{e}}/\langle \Delta E\rangle_{\mathrm{n}} \approx m_{\mathrm{n}}/Z_2 m_{\mathrm{e}}0 \gg 1$, and that the energy loss is proportional to v^{-2}, i.e. E^{-1}.

24.3.1 Elastic Collisions

The calculation of the energy loss in elastic collisions is complicated owing to the electron clouds screening the ion and target nuclei. The interaction potential is the product of a spherically symmetric screening function and the Coulomb potential Q_1/r. There are many different formulations for the screening function [9]. See Appendix 24.B for interatomic potentials. Using an appropriate screening function, the nuclear stopping of any ion in any target material can be evaluated analytically [15].

For a potential V, center-of-mass energy E_{c}, and impact parameter p, the final angle of scatter is obtained from the scattering integral:

$$\theta = \pi - 2p\int_{r_{\min}}^{\infty} r^{-2}\left[1 - \frac{V(r)}{E_c} - \frac{p^2}{r^2}\right]^{-1/2}\mathrm{d}r\,. \tag{24.8}$$

For an ion at energy E_0, the average energy transferred, namely the nuclear stopping cross section, is obtained by summing over all impact parameter values see (24.1) and (24.2):

$$S_{\mathrm{n}}(E_0) = 2\pi\eta E_0 \int_0^{p_{\max}} \sin^2 \frac{\theta}{2} p \, \mathrm{d}p \; . \tag{24.9}$$

In computer simulations using the BCA and MD techniques, an explicit analytical form for S_{n} is not needed. The nuclear energy loss is obtained directly from the interaction potential between the ion and the atoms.

The impinging ions produce recoil atoms, which produce new recoils and so forth. The energy lost in the collisions goes into heat and deformation of the material in which the slowing down occurs, as the atoms spread the kinetic energy in a series of collisions, namely in collision cascades.

24.3.2 Inelastic Collisions

Electronic stopping is the main source of energy loss for ions moving faster than v_{B} (see Fig. 24.1). There are several mechanisms contributing to the electronic stopping at ion velocities where relativistic effects can be neglected: (s1) momentum exchange in a collision between the ion and a free electron in the target material, (s2) ionization of the ion, (s3) capture of an electron by the ion, (s4) excitation of the ion, (s5) excitation of a target atom, (s6) ionization of a target atom, and (s7) collective effects such as polarization and plasmon excitation.

The electronic stopping takes place both during the collision of the ion and atom and between these collisions. Between the collisions, a constant slowing force acts on the ion owing to momentum exchange with the electrons in the material (s1). The stopping during a close collision of the ion and atom is connected to electron exchange between them (s4 and s5). In addition to these frozen-charge energy losses, there are charge-exchange events (s2, s3, and s6). The relative importance of the different contributions to the total electronic stopping power depends on the ion velocity [3]. There are three velocity regions: the high-velocity region for $v > v_{\mathrm{B}} Z_1^{2/3}$; the low-velocity region for $v < v_{\mathrm{B}}$, where the upper limit is the Bohr velocity of the target electrons or, in the electron gas theory, the Fermi velocity v_{F}; and the intermediate-velocity region for $v_{\mathrm{B}} < v < v_{\mathrm{B}} Z_1^{2/3}$. The velocity $v_{\mathrm{B}} Z_1^{2/3}$ is the mean velocity of the electrons filling the levels of a neutral atom with nuclear charge Z_1, as obtained from the Thomas–Fermi statistical theory [15].

For high ion velocities, Bohr calculated the stopping cross section for electron scattering from a moving ion (see [16]). A quantum-mechanical model by Bethe [7,17] is used for a fully stripped ion. In collisions with single electrons, the energy transferred to an electron $\Delta E(p)$, corresponding to electron excitation, results in the electronic stopping cross section

$$S_{\mathrm{e}}(E_0) = 2\pi \int_{p_{\min}}^{p_{\max}} \Delta E(p) p \, \mathrm{d}p = 4\pi \frac{Z_1^2 e^4}{m_{\mathrm{e}} v_0^2} \int_{p_{\min}}^{p_{\max}} \frac{\mathrm{d}p}{p} \, , \tag{24.10}$$

according to (24.1) and (24.3). A calculation based on the Born approximation gives the stopping power [7]

$$-\left(\frac{\mathrm{d}E}{\mathrm{d}x}\right)_{\mathrm{e}} = \frac{4\pi Z_1^2 e^4 N_{\mathrm{n}} Z_2}{m_{\mathrm{e}} v^2} \ln \frac{2 m_{\mathrm{e}} v^2}{I} \, , \tag{24.11}$$

where I is the mean excitation energy for the atom in its ground state.

Bethe's model [7] and correction terms arising from the shell corrections [18,19], the Bloch correction [20], the polarization effect [21] (or Barkas effect or Z_1^3 contribution), and relativistic effects [22] give an extensively used analytical description of the stopping. Owing to the needs of ion beam analysis, the electronic stopping power has been much studied at high ion velocities. The studies have resulted in accurate stopping tables for many ions in different materials.

At low velocities, the electronic stopping power involves mainly the mechanisms s1, s4, and s5. The most important one is s1 [15]. The theoretical description has been improved during the last two decades by nonlinear electron gas models. The main reason for the interest in the stopping power in this velocity region is the extensive use of ion implantation in the semiconductor industry.

The early model by Firsov [5] described the electronic stopping by the local transfer of energy from electrons of the ion to electrons of the atom. The retarding force acting on the ion leads in a change of the momentum. The electrons return when the ion moves away, but there is no back transfer of momentum because the electrons fall into higher energy levels. The electronic stopping cross section for media where atoms are located randomly is obtained from the energy transferred in one interaction between two atoms by integrating over all possible impact parameters, as in (24.10).

In binary collisions, the scattering angles are affected by the inelastic energy loss. The scattering angle is an average of the scattering angles before and after the collision. The scattering angle before the collision is given by (24.8), and after the collision by a similar integral but with a reduced energy and impact parameter [10].

In modern electronic-stopping calculations, the medium in which slowing down occurs is described as an electron gas or plasma with a constant density, and the ion is a perturbation in the gas [9]. The semiclassical analysis of the perturbation model uses Poisson's equation for a charge interacting with a polarizable medium characterized by a dielectric function [15]. The stopping integrals in the dielectric formalism [23] are calculated using Lindhard's linear approximations for the dielectric function both for slow and fast ions.

In the model by Lindhard and Scharff [6], the energy loss of an ion is proportional to the velocity:

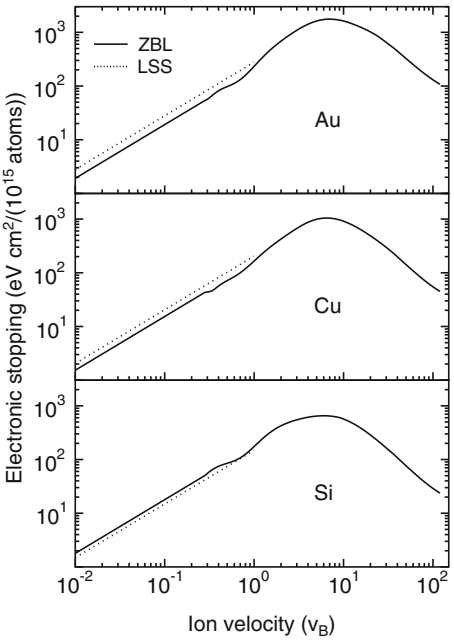

Fig. 24.2. Electronic stopping powers for silicon ions slowing down in silicon, copper, and gold. The LSS values have been calculated only up to v_{B}. For the ZBL values, see [9]

$$S_{\mathrm{e}}(E) = \xi_{\mathrm{e}} 8\pi e^2 a_{\mathrm{B}} \frac{Z_1 Z_2}{Z} \frac{v}{v_{\mathrm{B}}} \,, \tag{24.12}$$

where $Z = (Z_1^{2/3} + Z_2^{2/3})^{3/2}$ and $\xi_{\mathrm{e}} \approx Z_1^{1/6}$ (see Fig. 24.2). The first general model for the nuclear and electronic stopping of an ion was presented in 1963 by Lindhard et al. [3], who based their treatment of atoms on the statistical Thomas–Fermi atom model. The LSS model gives analytical formulas for the nuclear and the electronic stopping of any ion in any target material in the low-velocity region.

Most of the theories for electronic stopping at low energies use the local-density approximation. It is assumed that each volume element in the solid is an independent, free plasma with an electron density. The electronic stopping power is position-dependent and proportional to the velocity of the ion; $S_{\mathrm{e}} = \int I(v,\rho) Z_1^{\star}(v)^2 \rho \, \mathrm{d}V$, where $I(v,\rho)$ is the stopping interaction function of an ion of unit charge, $\rho(r)$ is the electron gas density or the electron density of the material in which slowing down occurs, and $Z_1^{\star}(v)$ indicates that the charge of the ion differs from the atomic number and depends on the velocity. Various expressions for the electronic stopping power depend on the description of the plasma in the solid (e.g. [24]).

In the intermediate-velocity region, ions lose and capture electrons. This velocity region is the most difficult one to describe theoretically, because all the mechanisms s1–s7 have to be evaluated. The heavier the ion is, the more electrons participate in the exchange processes. The stopping power depends strongly not only on the ion velocity but also on the atomic numbers of the ion and target atoms [25]. The stopping power is affected by the fact that the quantum states of the electrons are different for different atoms. The electron capture and loss processes (s2 and s3) can have a notable contribution to the stopping.

By using an empirical scaling rule, the stopping power for a heavy ion (HI) is obtained from the stopping for a proton (H) at the same velocity. The stopping power is factorized into the electronic stopping for the proton and the effective charge of the heavy ion:

$$S_{\mathrm{HI}} = S_{\mathrm{H}}(Z^{\star}_{\mathrm{HI}})^2 = S_{\mathrm{H}}(Z_{\mathrm{HI}}\gamma)^2 \,, \tag{24.13}$$

where Z_{HI} is the atomic number of the heavy ion and γ is its fractional effective charge. The fractional effective charge is defined such that the effective charge of the ion $Z^{\star}_1(v, Z_2)$ at a velocity v in the medium (Z_2) is $\gamma = Z^{\star}_1(v, Z_2)/Z_1(v, Z_2)$. The fractional charge of a proton is equal to one. Many different Z_1- and Z_2- dependent formulations have been proposed in the literature for the heavy-ion fractional effective charge [9, 26–30]. Sigmund and Schinner emphasize [11] that the significance of static projectile screening is heavily overestimated in conventional effective-charge theory.

The analytical models have typically predicted the stopping power by interpolating between the Bethe formula above and linear models below the stopping maximum. The model by Brandt and Kitagawa [8] provides a description frequently used for the stopping power of a partially ionized heavy ion. According to the BK model, the energy loss increases for small impact parameters owing to reduced screening.

For the energy loss of intermediate-velocity heavy ions in electronic plasma, Ziegler, Biersack, and Littmark [9] constructed a model (ZBL) based on the ideas of the BK model [8]. The stripping of electrons in a heavy ion is calculated by comparing the ion's electron velocities with the relative velocity v_{r} between the ion and the electronic velocity of the medium. For a known charge state, the electron distribution of the ion $\rho(r) = (N/4\pi\Lambda^3)(\Lambda/r)\exp(-r/\Lambda)$ is defined, with a screening length $\Lambda = 2a_{\mathrm{B}}(1-q)^{2/3}/[Z_1^{1/3}(1-(1-q)/7)]$. N is the number of electrons remaining in the ion. The fractional ionization $q = (Z_1 - N)/Z_1$ was deduced for heavy ions in an extensive data analysis to be $q = 1 - \exp\sum[a_i(v_{\mathrm{r}}/v_{\mathrm{B}}Z_1^{2/3})]^{b_i}$, where the constants a_i and b_i were obtained by fitting experimental data. The effective charge to be used in the calculation of the stopping power according to (24.13) is obtained from the fractional ionization

$$\gamma = q + 0.5(1-q)\left(\frac{v_{\mathrm{B}}}{v_{\mathrm{F}}}\right)^2 \ln\left[1 + \left(2\frac{\Lambda v_{\mathrm{F}}}{a_{\mathrm{B}}v_{\mathrm{B}}}\right)^2\right] \,. \tag{24.14}$$

The ZBL parametrization predicts empirically the stopping of any ion in any target material (see Fig. 24.2). Since the Fermi velocity has a constant value for each target material, the ion velocity and atomic number are the only parameters in the stopping function. Owing to several fitted parameters, the predicted electronic stopping powers are reasonably accurate, but the nonlocality limits the validity and accuracy for stopping calculations in crystalline structures in cases where channeling of ions (see Sect. 24.4.5) takes place.

24.4 Atomic Collisions in Matter

24.4.1 Energy Straggling

Ions are deflected and slowed down in matter by scattering from electrons and nuclei of substrate atoms. In implantation and irradiation experiments, there are many ion trajectories involved. The transport equations are the basis for analytical descriptions of ion penetration in solids. If an ion bombardment has a distribution of ions $F(\mathbf{r}, \mathbf{v}, t)$, where $\mathbf{r}$ and $\mathbf{v}$ are the position and velocity vectors, respectively, of the ions at time t, the forward form of the transport equations, namely the Boltzmann equation, is [10]

$$\frac{\partial F(\mathbf{r}, \mathbf{v}, t)}{\partial t} = -\,\mathbf{v} \cdot \nabla F(\mathbf{r}, \mathbf{v}, t) - N\mathbf{v}F(\mathbf{r}, \mathbf{v}, t) \int \mathrm{d}\mathbf{v}'\, \sigma(\mathbf{v}, \mathbf{v}') + N \int \mathbf{v}' \mathrm{d}\mathbf{v}'\, F(\mathbf{r},\mathbf{v}', t)\sigma(\mathbf{v}', \mathbf{v}) + \mathcal{S}(\mathbf{r}, \mathbf{v}, t)\,. \qquad (24.15)$$

$F(\mathbf{r}, \mathbf{v}, t)\,\mathrm{d}\mathbf{r}\,\mathrm{d}\mathbf{v}$ is the probability to find an ion in the volume $(\mathbf{r}, \mathrm{d}\mathbf{r})$ moving with velocity $(\mathbf{v}, \mathrm{d}\mathbf{v})$ at time t, $\sigma(\mathbf{v}, \mathbf{v}')$ is the cross section for scattering from $\mathbf{v}$ to $(\mathbf{v}', \mathrm{d}\mathbf{v}')$, and $\mathcal{S}(\mathbf{r}, \mathbf{v}, t)$ represents the distribution of ions arriving in the sample.

For the case where the ions pass through a thin foil with small energy losses and negligibly small deflections, the one-dimensional function $\phi(z, E)$ representing the number of ions traversing the foil, of thickness z, with a constant velocity E_0 is

$$\frac{\partial \phi(z, E)}{\partial z} = -\,\phi(z, E)N \int \mathrm{d}T\, \sigma(E, T) + N \int \mathrm{d}T\, \sigma(E + T, T)\phi(z, E + T) + \phi_0 \delta(z)\delta(E - E_0)\,, \qquad (24.16)$$

where the first integral refers to the energy before the collision, the second integral refers to the final energy, and the last term is the energy distribution of the incoming ions.

For a strongly peaked scattering cross section at a small energy loss, i.e. $\sigma(E+T,T) = \sigma(E,T)$, the integral can be given to first order, where the stopping is $S(E) = \int \mathrm{d}T\, T\sigma(E,T)$ and the straggling is

$$\Omega^2(E) = \int \mathrm{d}T\, T^2\sigma(E,T)\ , \tag{24.17}$$

by the equation

$$\frac{\partial\phi(z,E)}{\partial z} = NS(E_0)\frac{\partial\phi(z,E)}{\partial E} + \frac{N\Omega^2(E_0)}{2}\frac{\partial^2\phi(z,E)}{\partial E^2}\ . \tag{24.18}$$

The solution with the boundary condition $\phi(0,E_0) = \phi_0\delta(E-E_0)$ results in the Gaussian approximation describing the spectra of ions traversing a thin film and losing an energy $\Delta E = E_0 - E$,

$$\phi(z,\Delta E) = \frac{\phi_0}{[2\pi zN\Omega(E_0)]^{1/2}}\exp\left(-\frac{[\Delta E - zNS(E_0)]^2}{2zN\Omega(E_0)}\right)\ . \tag{24.19}$$

After traversing a distance Δz in matter and losing energy as given by (24.7), the ions have a straggling

$$\Omega^2_{\mathrm{n/e}} = N\,\Delta z\, 4\pi(Z_1e)^2(Z_2e)^2\frac{m^2_{\mathrm{ion}}}{(m_{\mathrm{ion}}+m_{\mathrm{n/e}})^2}\left(1-\frac{T_{\min}}{T_{\max}}\right) \tag{24.20}$$

owing to elastic collisions with nuclei (n) and inelastic collisions with electrons (e). For heavy ions, the nuclear contribution is sizable.

In the region of high ion velocity, the straggling is almost independent of projectile velocity and is given by the formula derived by Bohr [31, 32],

$$\Omega^2_{\mathrm{B}}[\mathrm{keV}^2] = 0.26Z_1^2Z_2N\,\Delta z[10^{18}\mathrm{at./cm}^2]\ . \tag{24.21}$$

This straggling formula has been improved by many authors to extend its applicability to lower velocities of light ions. Lindhard and Scharff [33] proposed a correction for low ion velocities. Yang et al. [34] summarized the development of straggling calculations [35–44], undertook a survey of H, He, and heavy-ion straggling data, and developed a fitting function for the Chu model [36]. By use of the effective charge and a scaling approach for energy straggling and considering correlation and charge-exchange effects, functions were obtained for heavy-ion straggling.

24.4.2 Multiple Scattering

In collisions with nuclei and electrons, the ions undergo scattering, as demonstrated in Fig. 24.3. The average deflection is zero because of symmetry,

but the average square deflection is finite and results in an angular divergence of the ion beam. The angle of scattering θ given in center-of-mass coordinates in (24.5) transforms, in laboratory coordinates, to $\phi = \tan^{-1}[m_2 \sin\theta/(m_1 + m_2 \cos\theta)]$. The average square deflection for small scattering angles, analogously to (24.17), is

$$\langle \Phi^2 \rangle = N \, \Delta z \int \phi^2 \, \mathrm{d}\sigma \, , \tag{24.22}$$

where the integral goes from zero to a maximum value of the angle. If the probability of wide-angle scattering is assumed to be negligible, the angular spread of the ions is related directly to the stopping power, i.e. $\langle \Phi^2 s \rangle \approx N \, \Delta z (m_2/m_1 E) S(E)$. The angular distribution of the ion beam can be approximated by a Gaussian form,

$$F(\Phi) = \frac{1}{(2\pi \langle \Phi^2 \rangle)^{1/2}} \exp\left(-\frac{\Phi^2}{2\langle \Phi^2 \rangle} \right) \, . \tag{24.23}$$

These equations have to be modified to take into account the large-angle scattering due to the nuclear stopping power. Early theoretical work on small-angle scattering of ions has been summarized in [45]. To meet the needs of experiments, the theory was further developed by Sigmund et al. [46–48] and, very recently, in [49].

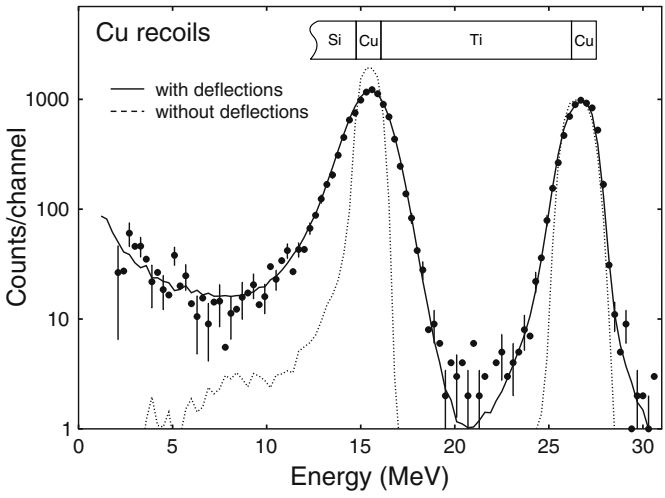

Fig. 24.3. Multiple scattering of Cu recoils in titanium as observed in TOF-ERDA measurements [60]. The Cu recoils were produced by bombardment of 23 nm thick Cu marker layers on the surface of a 200 nm thick Ti foil and at the interface between the Ti foil and Si substrate by 53 MeV $^{127}I^{10+}$ ions. The dots are experimental values. The simulated spectrum without scattering but with energy straggling is indicated by "without deflections", and the simulated spectrum with the scattering by "with deflections"

24.4.3 Z_1 and Z_2 Oscillations

In comparisons of experimental stopping data with the predictions of the theories of Firsov [5] and Lindhard and Scharff [6], the experimental data showed an oscillatory structure in the stopping power vs. Z_1 [50–54]. The Z_1 dependence is enhanced under channeling conditions, under which the moving particle experiences glancing collisions with the lattice atoms at an almost constant impact parameter. A number of investigations have dealt with models with the aim of explaining the oscillatory structure, including [50–56].

The electron shells were explained to be the reason for the fluctuation of the stopping of an ion (Z_1) as a function of the material in which slowing down occurs (Z_2) and for the fluctuation of the stopping in a given material for different ions [56–59]; these functions are called Z_2 and Z_1 oscillations, respectively (see Fig. 24.4).

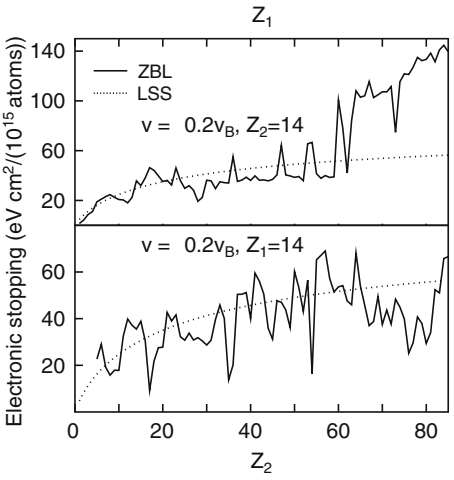

Fig. 24.4. Electronic stopping powers in different materials illustrating the Z_1 and Z_2 oscillations; for the ZBL values, see [9]

According to the model by Echenique et al. [56], the Z_1 oscillations can be taken into account by including a momentum-transfer cross section σ_{tr} in the equation for the low-energy stopping power of a free-electron gas $S_{\mathrm{e}}(v) = nvv_{\mathrm{F}}\sigma_{\mathrm{tr}}(v_{\mathrm{F}})$, where nv is the uniform current of electrons scattered by a screened potential and $v_{\mathrm{F}}\sigma_{\mathrm{tr}}$ is the integrated scattering rate. The final expression for the stopping power depends on the approximation used for σ_{tr}. For a spherically symmetric scattering potential the stopping cross section is [56]

$$S_{\mathrm{e}}(v) = \frac{3v}{k_{\mathrm{F}} r_{\mathrm{s}}^3} \sum_{l=0}^{\infty} (l+1) \sin^2(\delta_l(E_{\mathrm{F}}) - \delta_{l+1}(E_{\mathrm{F}})) \,, \tag{24.24}$$

where $r_{\mathrm{s}} = [3/(4\pi n)]^{1/3}$ is a measure of the electron density defined as the radius of a sphere whose volume is equal to the volume per conduction electron, and $\delta_l(E_{\mathrm{F}})$ represents the scattering phase shifts of electrons scattered by the effective potential of the atom for the lth partial wave in the expansion of the electron wave function. Echenique and coworkers defined, in an operational manner, an effective charge $Z_1^{\star} = [(\mathrm{d}E/\mathrm{d}x)_{Z>1}/(\mathrm{d}E/\mathrm{d}x)_{\mathrm{proton}}]^{1/2}$. Using the density-functional approach and the effective charge, they succeeded in scaling the electronic stopping powers for $Z_1 \geq 2$ particles to that of protons.

When the electronic stopping for channeled ions is plotted versus the atomic number of the target material Z_2, it shows oscillations similar to those for Z_1. On the basis of experimental data, Brandt and Kitagawa [8] concluded that a comprehensive description of low-velocity electronic stopping powers could be given if reference is made not to Z_2 but to the valence electron density.

24.4.4 Compound Materials

Bragg's rule [61] states that the stopping power of a compound target is the weighted average of the atomic stopping powers of the constituents $S = \sum a_i S_i$, where the sum of the weights a_i describing the fractions of the atoms in the compound is equal to one. Deviations from this rule occur owing to differences in the electronic structure between a free atom and an atom bound in a molecule or an alloy. Consequently, deviations from the rule should be expected at low energies, where the relative contribution from valence electrons to the stopping power is large, and for very light elements, where the valence electrons constitute a major fraction of the total number of electrons. The deviations are most pronounced, about 10–20%, around the stopping maximum for light organic gases and for solid compounds containing heavier constituents, such as oxides and nitrides. In an empirical model [62], two contributions are assumed, the effect of the closed electron shells of atoms and the effect of the chemical bonds. The average accuracy of the calculations obtained was better than 2% for compounds with known bond structures.

24.4.5 Effects of the Crystalline Structure of Matter

The crystalline structure of the target material has a large effect on the stopping [63, 64]. The periodicity in the structures of crystalline materials forms channels for the impinging ions. The atom and electron densities have lower values in the channels than in the bulk. The electron density can be several decades lower in the middle of a channel than near a nucleus. Thus the contribution to the stopping from the bound electrons is less important

in channels. The low atom and electron densities lead to lower nuclear and electronic stopping powers, respectively, in the channels than elsewhere in the bulk.

There are two different approaches to calculating the electronic stopping in channels, namely methods based on the binary-collision approximation (BCA), with the impact parameter as a variable, and MD calculations, using the local electron density as the variable. The benefit of BCA calculation is that the different stopping contributions are well separated by the use of cross sections and are straightforward to calculate. MD calculations have the advantage of using an accurate local electron density inside the material and the possibility of including many-body collisions.

Stopping powers in channels have been calculated by MD simulations using models based on the BK theory [65, 66] and spherical charge densities for the target atoms. The effective charge of an ion was calculated using a fitted Fermi velocity for the material as the only free parameter. Owing to the fitted values, the model gives very good results for channeled low-energy ions. The results were improved in [67] by the use of a more accurate three-dimensional electron density distribution for crystalline silicon to obtain the local electron density and local Fermi velocity inside the crystal.

24.5 Collision Cascades and Implantation-Induced Damage

In noninsulating materials, the damage in a collision cascade is produced mainly by the nuclear energy deposition. In insulators, the electronic energy loss can also contribute to the production of atomic damage, although the detailed mechanisms for this are not fully understood.

In materials consisting of light atoms and having a low atomic density, such as silicon, the cascades are roughly linear and no large liquid zones form within the cascade. The cascade development and damage distribution can be represented rather well by BCA simulations, especially if the parameters in the simulation are calibrated with MD simulations [68]. In semiconductor materials, regions of the crystal can become strongly disordered by the irradiation, forming amorphous zones upon cooling down owing to the low recrystallization rate of these materials [69]. In heavy, dense metals, large liquid zones formed during irradiation are recrystallized almost perfectly during the cooling-down phase of the cascade and only a few isolated point defects remain [70,71]. The total damage production at keV energies is about a factor of five less than expected from a linear cascade model [72, 73].

Surface effects in collision cascades induced by a single ion are divided into four categories. The first effect, sputtering of single recoil atoms by ballistic collisions (Fig. 24.5a), is well understood from classical theory [74, 75] and simulations (see e.g. [76–81]). For light materials and ions penetrating deep into the sample, sputtering can be the only surface effect of a cascade. In

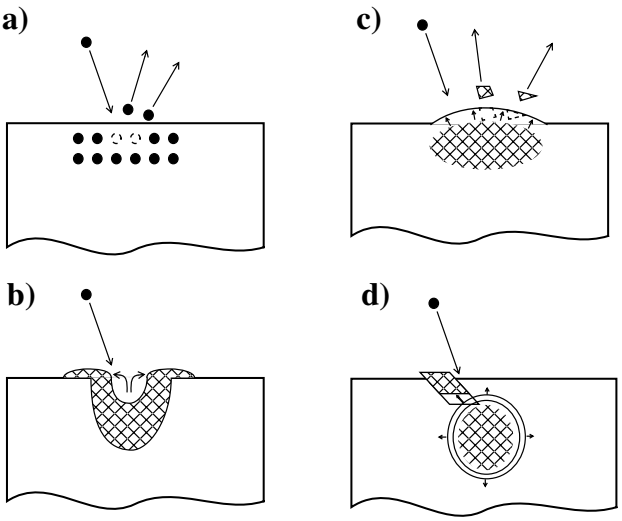

Fig. 24.5. Different mechanisms for ion-irradiation-induced damage close to the surface. (**a**) sputtering of single recoil atoms by ballistic collisions, (**b**) plastic flow of hot liquid onto the surface, (**c**) microexplosions, and (**d**) coherent displacement of atoms

dense materials, the collisions produced by a heavy ion, typically at an energy of a few keV, can be so well localized that they can produce a liquid-like zone inside the material or close to the surface [70]. The other three surface effects all require that such a zone is formed somewhere in the cascade. The second effect, plastic flow of hot liquid onto the surface, can result when a cascade is centered inside the sample, but is bounded by the surface so that liquid atoms can flow onto the surface (Fig. 24.5b) [82]. The third effect, "microexplosions", occurs when the liquid zone is so close to a surface that the pressure wave from the cascade essentially ruptures the surface (Fig. 24.5c). In this case, pockets of hot liquid can explode out from the surface as a direct result of the collision cascade [80,83]. The fourth kind of surface damage effect is a coherent displacement of atoms, leading to the formation of an adatom island (Fig. 24.5d) [84].

The microexplosion effect corresponds to the nonlinear sputtering regime, and has thus been indirectly observed in numerous experimental sputtering studies. It is expected to produce craters on the sample surface, which have been observed in several experiments [85,86]. A recent comparison of simulations and experiments has shown that the observed crater formation can be explained by the liquid flow and microexplosion mechanisms [83,87].

24.A Appendix: Computer Methods to Calculate the Slowing Down of Ions

24.A.1 Binary-Collision Approximation Method

Analytical calculations of binary collisions have been used to deduce the stopping power as a function of the ion velocity. Computer simulations which treat the successive collisions as binary collisions are called binary-collision approximation (BCA) [88] methods. These methods are based on Monte Carlo (MC) techniques. One of the main tools in the field of statistical particle penetration has been the use of transport equations and MC techniques to solve them numerically [15]. Particle penetration was one of the first major applications of computer simulations in physics [15].

In the MC technique, a random number is used to determine the free-flight path l of an ion from an exponential distribution $F(l) = (1/\lambda)\mathrm{e}^{-l/\lambda}$, where $\lambda = 1/(N\sigma(E))$ is the mean free path, N is the atom density of the target, and $\sigma(E)$ is the cross section for all possible collisions under consideration. The type of a collision is defined by a random number, resulting in a changed path for the ion, namely a new direction, charge state, energy, etc. Each collision is treated as binary, neglecting the rest of the environment. This procedure is then iterated until the ion has lost all of its energy. The implantation of ions is simulated by following the ions until they stop, and a histogram of the penetration depths from the target surface is used to give the range profile of the ions.

An MC calculation is very fast with modern computers, requiring typically seconds or minutes of total simulation time. There are several BCA codes [77, 89–91] available, of which the code most often used is TRIM [91] and later parametrizations of it [9].

24.A.2 Molecular-Dynamics Method

In the molecular-dynamics (MD) method, the movement of the ion is simulated more accurately than in the BCA methods. There are two factors behind the better accuracy: (i) the properties of the target structure can be described more realistically, and (ii) the ion can interact with several atoms at a time.

In MD simulations, the atoms in the system are given initial spatial and momentum coordinates. By solving the Newtonian equations of motion in a small time step for all the atoms, the atomic coordinates are changed. This process is then iterated until the given criterion (for example the maximum time) for the termination of the simulation is fulfilled. The accuracy of the ion movement depends on the length of the time step. The movement of the atoms is determined by the forces acting between them. The forces depend on the interaction potentials of the atoms, which are usually divided into repulsive and attractive parts.

The MD method makes it possible to include all the many-body collisions neglected in the BCA simulations. Thus it is the only way to calculate ion movement for low energies or in the case of atom-cluster implants. The electronic structure of the target material can also be constructed accurately, because the spatial coordinates of all atoms in the simulation are determined during every time step.

A full MD simulation is very computer-time-consuming, and this limits its use to very low energies (<1 keV/amu). Different methods have been developed to limit the calculations only to the vicinity of the moving ion (e.g. [66,92]). Thus the simulation time with normal desktop computers needs only to be from minutes to hours for statistically significant results. The drawback is that the cascades are not taken into account, which means that the change in the target structure cannot be calculated directly.

24.B Appendix: Interatomic Potentials

The forces between atoms define not only the scattering of an incoming ion by an atom of matter but also almost all physical and chemical phenomena in matter. The forces are derived from an interatomic-potential model function V depending on the positions of the atoms. For a system of N atoms whose position vectors are $\mathbf{r}_i$, the force $\mathbf{F}_i$ on the ith atom is given by $\mathbf{F}_i = -\partial V(\mathbf{r}_1, \mathbf{r}_2, \ldots, \mathbf{r}_N)/\partial \mathbf{r}_i$.

For the case of two atoms, $\mathbf{F} = -\partial V(\mathbf{r})/\partial \mathbf{r}$, where $\mathbf{F}$ is the force acting on either of the particles, whose mutual separation is $\mathbf{r}$. For two-body interactions it can be assumed that $V \to 0$ as $r \to \infty$ and that $V(r) \sim 1/r$, and, owing to the strong nuclear repulsion, $V \to \infty$ as $r \to 0$.

The interatomic force is defined by a screened Coulomb potential

$$V = \frac{Z_1 Z_2 e^2}{r} \chi(r/a_0) \,, \tag{24.25}$$

where the screening function is $\chi(r/a_0)$. It is given as a function of distance in units of $a_0 = 0.8853 a_\mathrm{B} Z^{-1/3}$, where a_B is the Bohr radius. Several screening functions have been reported in the literature (see Fig. 24.6). These include the function given by Bohr, $\chi(x) = \mathrm{e}^{-x}$; the Thomas–Fermi function, $\chi(x) = [1 + (x^3/144)^{0.8034/3}]^{(-3/0.8034)}$; the Molière function, $\chi(x) = 0.35\mathrm{e}^{-0.3x} + 0.55\mathrm{e}^{-1.2x} + 0.10\mathrm{e}^{-6.0x}$; and the Lenz–Jensen function, $\chi(x) = \mathrm{e}^{-q}(1 + \sum a_i q_i)$, where $q = 3.11126 x^{1/2}$.

In computer simulation codes, the standard semiempirical interatomic-potential function (ZBL) [9] $\chi(x) = \sum a_i \mathrm{e}^{-b_i x}$ is conventionally used. The values of the coefficients have been obtained by fitting to quantum mechanically calculated data.

At distances of around 0.1–0.4 nm, the interatomic potential is attractive. The properties of diatomic molecules, binding energies, and equilibrium

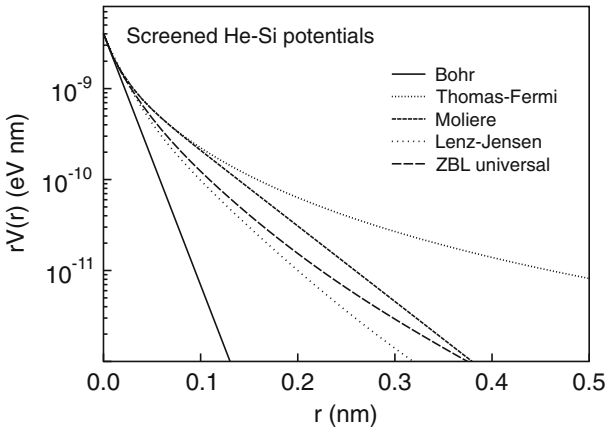

Fig. 24.6. Screening function for different potentials [9]

separations, as well as the properties of matter at and close to thermal equilibrium, are determined by a potential containing a repulsive and an attractive part.

References

1. N. Bohr: Phil. Mag. **25** (1913) 16
2. N. Bohr: Phys. Rev. **58** (1940) 654
3. J. Lindhard, M. Scharff, H. E. Schiøtt: Mat. Fys. Medd. Dan. Vid. Selsk. **33** (1963) 1
4. E. Fermi, E. Teller: Phys. Rev. **72** (1947) 399
5. O. Firsov: Sov. Phys. JETP **9** (1959) 1076
6. J. Lindhard, M. Scharff: Phys. Rev. **124** (1961) 128
7. H. Bethe: Ann. Phys. **5** (1930) 324
8. W. Brandt, M. Kitagawa: Phys. Rev. B **25** (1982) 5631
9. J. F. Ziegler, J. P. Biersack, U. Littmark: *The Stopping and Range of Ions in Matter*, Pergamon, New York, 1985. The computer program SRIM is based on this ZBL parametrization of the electronic stopping power. The version SRIM2003.24 has been used in this chapter
10. R. Smith, M. Jakas, D. Ashworth, B. Owen, M. Bowyer, I. Chakarov, R. Webb (eds.): *Atomic and Ion Collisions in Solids and at Surfaces*, Cambridge University Press, Cambridge, 1997
11. P. Sigmund, A. Schinner: Nucl. Instr. Meth. Phys. Res. B **195** (2002) 64
12. N. R. Arista: Nucl. Instr. Meth. Phys. Res. B **195** (2002) 91; see also erratum: Nucl. Instr. Meth. Phys. Res. **207** (2003) 232.
13. P. L. Grande, G. Schiwietz: Nucl. Instr. Meth. Phys. Res. B **195** (2002) 55
14. P. Sigmund: Phys. Scr. **28** (1983) 257
15. A. Gras-Marti, H. M. Urbassek, N. Arista, F. Flores (eds.): *Interaction of Charged Particles with Solids and Surfaces*, Plenum; New York, 1991

16. P. Sigmund, A. Schinner: Eur. Phys. J. D **12** (2000) 425
17. P. Sigmund, A. Schinner: Eur. Phys. J. D **15** (2001) 165
18. J. R. Sabin, J. Oddershede: Phys. Rev. A **26** (1982) 3209
19. J. R. Sabin, J. Oddershede: At. Data Nucl. Data Tables **31** (1984) 275
20. H. Bichsel: Phys. Rev. A **65** (2002) 52709
21. J. M. Pitarke, R. H. Ritchie, P.M. Echenique: Phys. Rev. B **52** (1995) 13883
22. E. Uggerhøj: Phys. Scr. **28** (1983) 331
23. D.G. Arbo, J.E. Miraglia: Phys. Rev. A **58** (1998) 2970
24. P. M. Echenique, I. Nagy, A. Arnau: Int. J. Quantum Chem. **23** (1989) 521
25. P. Sigmund, A. Fettouhi, A. Schinner: Nucl. Instr. Meth. Phys. Res. B **209** (2003) 19
26. L. Nortcliffe, R. Schilling: Nucl. Data Tables **7** (1970) 233
27. J. Forster, D. Ward, H. Andrews, G. Ball, G. Costa, W. Davies, I. Mitchell: Nucl. Instr. Meth. **136** (1976) 349
28. J. Anthony, W. Lanford: Phys. Rev. A **25** (1982) 1868
29. F. Hubert, R. Bimbot, H. Gauvin: At. Data Nucl. Data Tables **46** (1990) 1
30. J. F. Ziegler: *Handbook of Stopping Cross-Sections for Energetic Ions in All Elements*, Pergamon, New York, 1980
31. N. Bohr: Mat. Fys. Medd. Dan. Vid. Selsk. **18** (1948) 8
32. N. Bohr: Mat. Fys. Medd. Dan. Vid. Selsk. **24** (1948) 19
33. J. Lindhard, M. Scharff: Mat. Fys. Medd. Dan. Vid. Selsk. **27** (1953) 15
34. Q. Yang, D. O'Connor, Z. Wang: Nucl. Instr. Meth. Phys. Res. B **61** (1991) 149
35. E. Bonderup, P. Hvelplund: Phys. Rev. A **4** (1971) 562
36. W. Chu: Phys. Rev. A **13** (1976) 2057
37. F. Besenbacher, J. Andersen, E. Bonderup: Nucl. Instr. Meth. **168** (1980) 1
38. M. Livingston, H. Bethe: Rev. Mod. Phys. **9** (1937) 245
39. L. Landau: J. Phys. USSRM **8** (1944) 201
40. P. Vavilov': Sov. Phys. JETP **5** (1957) 749
41. P. Schulek, B. Golovin, L. Kulyukina, S. Medved, P. Pavlovich: Sov. J. Nucl. Phys. **4** (1966) 996
42. C. Tschalaer: Nucl. Instr. Meth. **64** (1968) 237
43. H. Bichsel, R. Saxon: Phys. Rev. A **11** (1975) 1286
44. C. Sofield: Nucl. Instr. Meth. B **45** (1990) 648
45. W. Scott: Rev. Mod. Phys. **35** (1963) 231
46. P. Sigmund, K. Winterbon: Nucl. Instr. Meth. **119** (1974) 541
47. A. Marwick, P. Sigmund: Nucl. Instr. Meth. **126** (1975) 317
48. P. Sigmund, J. Heinemeier, F. Besenbacher, P. Hvelplund, H. Knudsen: Nucl. Instr. Meth. **150** (1978) 221
49. G. Amsel, G. Battistig, A. L'Hoir: Nucl. Instr. Meth. Phys. Res. B **201** (2003) 325
50. J. Ormrod, H. Duckworth: Can. J. Phys. **41** (1963) 1424
51. J. Ormrod, J. MacDonald, H. Duckworth: Can. J. Phys. **43** (1965) 275
52. J. Ormrod: Can. J. Phys. **46** (1968) 497
53. B. Fastrup, A. Borup, P. Hvelplund: Can. J. Phys. **46** (1968) 489
54. P. Hvelplund, B. Fastrup: Phys. Rev. **165** (1968) 408
55. K. Winterbon: Can. J. Phys. **46** (1968) 2429
56. P. M. Echenique, R. M. Nieminen, J. C. Ashley, R. H. Ritchie: Phys. Rev. A **33** (1986) 897

57. I. Nagy, A. Arnau, P. M. Echenique: Phys. Rev. A **40** (1989) 987
58. K. Shima, N. Kuno, M. Yamanouchi: Chin. J. Phys. **26** (1988) 292
59. G. de M. Azevedo, M. Behar, P. L. Grande: Phys. Rev. B **63** (2001) 64101
60. K. Arstila, T. Sajavaara, J. Keinonen: Nucl. Instr. Meth. Phys. Res. B **174** (2001) 163
61. W. Bragg, R. Kleeman: Phil. Mag. **10** (1905) 318
62. J. Ziegler, J. Manoyan: Nucl. Instr. Meth. Phys. Res. B **35** (1988) 215
63. I. Ruge, J. Graul (eds.):, *Ion Implantation in Semiconductors*, Springer, Berlin, 1971
64. S. Tian: J. Appl. Phys. **93** (2003) 5893
65. D. Cai, N. Grønbech-Jensen, C. M. Snell, K. M. Beardmore: Phys. Rev. B **54** (1996) 17147
66. K. M. Beardmore, N. Grønbech-Jensen: Phys. Rev. E **57** (1998) 7278
67. J. Sillanpää, K. Nordlund, J. Keinonen: Phys. Rev. B **62** (2000) 3109
68. H. L. Heinisch, B. N. Singh, T. Diaz de la Rubia: J. Nucl. Mat. **212–215** (1994) 127
69. M.-J. Caturla, L. A. M. T. Diaz de la Rubia, G. H. Gilmer: Phys. Rev. B **54** (1996) 16683
70. T. Diaz de la Rubia, R. S. Averback, R. Benedek, W. E. King: Phys. Rev. Lett. **59** (1987) 1930; see also erratum: Phys. Rev. Lett. **60** (1988) 76
71. K. Nordlund, M. Ghaly, R. S. Averback, M. Caturla, T. Diaz de la Rubia, J. Tarus: Phys. Rev. B **57** (1998) 7556
72. D. J. Bacon, T. Diaz de la Rubia: J. Nucl. Mat. **216** (1994) 275
73. R. S. Averback, T. Diaz de la Rubia: Displacement damage in irradiated metals and semiconductors, in: *Solid State Physics*, ed. H. Ehrenfest and F. Spaepen, volume 51, pp. 281–402, Academic Press, New York, 1998
74. R. Behrisch (ed.): *Sputtering by Particle Bombardment I*, Springer, Berlin, 1981.
75. P. Sigmund: Nucl. Instr. Meth. Phys. Res. B **27** (1987) 1
76. H. H. Andersen: Appl. Phys. **18** (1979) 131
77. W. Möller, W. Eckstein: Nucl. Instr. Meth. Phys. Res. B **2** (1984) 814
78. R. Smith, R. P. Webb: Nucl. Instr. Meth. Phys. Res. B **59/60** (1991) 1378
79. J. Likonen, M. Hautala: J. Phys. Condens. Matter **1** (1989) 4697
80. H. M. Urbassek, K. T. Waldeer: Phys. Rev. Lett. **67** (1991) 105
81. W. Eckstein, S. Hackel, D. Heinemann, B. Fricke: Z. Phys. D: At. Mol. and Clusters **24** (1992) 171
82. M. Ghaly, R. S. Averback: Phys. Rev. Lett. **72** (1994) 364
83. M. Ghaly, K. Nordlund, R. S. Averback: Phil. Mag. A **79** (1999) 79
84. K. Nordlund, J. Keinonen, M. Ghaly, R. S. Averback: Nature **398** (1999) 49
85. K. L. Merkle, W. Jäger: Phil. Mag. A **44** (1980) 741
86. S. E. Donnelly, R. C. Birtcher: Phys. Rev. B **56** (1997) 13599
87. M. Morgenstern, T. Michely, G. Comsa: Phil. Mag. A (1999) **79**
88. M. T. Robinson, I. M. Torrens: Phys. Rev. B **9** (1974) 5008
89. M. T. Robinson: Nucl. Instr. Meth. Phys. Res. B **67** (1992) 396
90. M. Hautala, I. Koponen: Defect Diffus. Forum **57–58** (1988) 61
91. J. P. Biersack, L. G. Haggmark: Nucl. Instr. Meth. **174** (1980) 257
92. K. Nordlund: Comput. Mater. Sci. **3** (1995) 448